Examining the effect of nanosized $Mg_{0.6}Ni_{0.4}O$ and Al_2O_3 additives on S/polyaniline cathodes for lithium–sulphur batteries

Assiya Yermukhambetova [a,b], Zhumabay Bakenov [b,c], Yongguang Zhang [c,d], Jawwad A. Darr [e], Daniel J.L. Brett [a], Paul R. Shearing [a,*]

[a] Electrochemical Innovation Lab, Department of Chemical Engineering, UCL, Torrington Place, London WC1E 7JE, UK
[b] Nazarbayev University, 53 Kabanbay Batyr Ave., Astana 010000, Kazakhstan
[c] Institute of Batteries LLC, 53 Kabanbay Batyr Ave., Astana 010000, Kazakhstan
[d] Tianjin Key Laboratory of laminating Fabrication & Interface Control Technology for Advanced Materials, Tianjin 300130, China
[e] Department of Chemistry, Christopher Ingold Laboratories, University College London, London WC1H 0AJ, UK

ABSTRACT

Nanostructured magnesium nickel oxide $Mg_{0.6}Ni_{0.4}O$ and alumina Al_2O_3 were studied as additives to sulphur/polyaniline (S/PANI) composites via wet ball-milling of sulphur and polyaniline followed by heat treatment. Metal oxide nanoparticles, which have small particle size, porous structure and high specific surface area to volume ratio, are expected to be catalytic for chemical reactions, including electron transfer and are able to adsorb lithium polysulphides. The composites were characterized by SEM and electrochemical methods. Cyclic voltammetry studies suggest that the alumina additive acts differently to the $Mg_{0.6}Ni_{0.4}O$. The results suggest that although the alumina additive improves the S/PANI composite performance as a lithium–sulphur battery cathode, the use of $Mg_{0.6}Ni_{0.4}O$ is more effective.

© 2015 The Authors. Published by Elsevier B.V. This is an open access article under the CC BY license (http://creativecommons.org/licenses/by/4.0/).

1. Introduction

Batteries based on lithium are some of the most promising electrochemical energy storage technologies available. This is due to their high energy density and prolonged cycle life compared with other rechargeable battery systems (Pb, Ni–Cd, Ni–MH). However, there are certain limitations in existing lithium ion battery (LiB) technologies, primarily related to their cost, safety and the limit of energy density which are not sufficient to meet electric vehicle battery requirements for extended ranges [1–3]. In order, among other things, to extend the range of electric vehicles, research is turning to the use of new chemistries based on Li-ion technology, which offer higher energy densities and high power: the lithium/sulphur (Li/S) battery is one such system, having a theoretical energy density of 1675 mA h g^{-1} [1] significantly higher than that of LIBs (372 mAh/g for a conventional graphite anode). Furthermore, elemental sulphur has the advantage of being both abundant and low cost [4,5]. However, despite the intensive attention of the electrochemistry community for many years, this system has not yet been commercialized due to critical limitations that have to be overcome: Li/S batteries suffer from rapid capacity fade and the practical capacity and cycle life of Li/S cells are usually lower than expected. This stems from the electrically insulating nature of sulphur and thus the low electrical conductivity of S electrodes; dissolution of lithium polysulfide intermediates that occur during battery cell charge/discharge; the large volume change during intercalation processes, ca. 80% due to reduction from elemental sulphur to Li_2S (density of S is 2.03 g cm^{-3}, whilst density of Li_2S is 1.66 g cm^{-3}) [4–7]; and deposition of non-soluble Li_2S on the surface of both cathode and anode.

Until now, a variety of techniques have been developed to improve the electrochemical performance of sulphur electrodes. The intrinsic low conductivity of sulphur can be enhanced by different approaches to form a continuous conductive path in the electrode, thus promoting rate capability and higher sulphur utilization.

Conducting polymers have gained extensive attention as a host or coating media for S cathodes due to their good environmental stability and conductivity as well as their useful mechanical properties. Along with the increase of conductivity, these polymers can encapsulate sulphur in their matrix. Another advantage of these polymers is their mechanical softness and 'self-healing' properties, that can help to address the S cathode volume change issue during charge–discharge [8,9].

Thus, conductive polymers such as polyacrylonitrile (PAN) [10–12], polypyrrole (PPy) [13–17], polythiophene [18] and recently polyaniline [19–22] have been used as additives in Li/S composite cathodes. It was shown that, along with the enhancement of the composite conductivity, the additive improves the homogeneity of sulphur distribution which positively affects the electrochemical performance of the cell.

Previously, Zhang et al. prepared a S/PPy composite by ball milling without heat treatment, thus avoiding sulphur loss due to sublimation; had relatively high discharge capacities of ca. 600 mA h g^{-1} after 20 cycles and 500 mA h g^{-1} after 40 [15]. Wang et al. [11] reported a S/PAN composite cathode material that exhibited a specific capacity of 850 mA h g^{-1} at the initial cycle and remained above 600 mA h g^{-1} after 50 cycles.

Polyaniline has been used as a coating agent prepared using an in situ chemical-oxidative-polymerization method and by simple ball milling and has demonstrated excellent performance as a conductive matrix. Polyaniline nanotube/S composite synthesized by Li et al. [22] showed a capacity of 837 mA h g^{-1} after 100 cycles at 0.1 C rate, with electrode stability up to 500 cycles at 1 C rate.

Inorganic ceramic fillers (oxides additives) such as $Mg_{0.6}Ni_{0.5}O$ [9, 20], Al_2O_3 [24–27], V_2O_5 [28], and TiO_2 [29] have also been employed to further improve the cathode conductivity and to prevent polysulphides shuttling into organic electrolytes by using them as adsorbents. In most of these studies the S/metal oxide composite was prepared by ball milling and heat treatment. Dong et al. [26] used a liquid phase preparation methodology for the S-Al_2O_3 composite preparation. The authors claimed that this technique allows homogenous mixing of Al_2O_3 in the composite electrode. It was demonstrated that Al_2O_3 can effectively 'trap' polysulphides and enhance the electrochemical performance of the Li/S cell. The initial discharge capacity of the cathode with the added alumina was 1171 mA h g^{-1}, and the remaining capacity was 585 mA h g^{-1} after 50 cycles at 0.25 mA cm^{-2}.

Song et al. [23] used $Mg_{0.6}Ni_{0.5}O$ prepared by a sol–gel method and demonstrated that this additive can improve the electrochemical performance and achieve an initial capacity of 1185 mA h g^{-1}. In earlier studies carried out by the authors [9,26], this approach was optimized by simplifying the preparation method and minimizing the amount of $Mg_{0.6}Ni_{0.5}O$ added up to 4 wt.%, and investigated its effect on conventional S and S/polyacrylonitrile (PAN) composite cathode performance. The initial capacity of these cathodes was 850 mA h g^{-1} and 1223 mA h g^{-1} at a constant current of 167.5 mA g^{-1} (0.1 C), respectively.

Herein we report on the comparative studies of the effect of two metal oxides on the S/polyaniline (PANI) composite cathode performance in lithium cell, both capacity and cycle life. There are various approaches that can be used to prepare a S/polymer composite, which include: a) coating by mixing conductive polymer and sublimed sulphur with further heat treatment, thus letting organo-sulphur bonds to be formed [12,15,19]; b) incorporation of the sublimed sulphur on polymer nanotubes [13,20]; c) in situ deposition of sulphur with conductive polymer [14,22]. In this work we have adopted the first approach due to its simplicity and ease of scale up features.

The addition of conductive polymers to composite cathode materials is thought to enhance the electrical conductivity, as well as the mechanical properties of the electrode, which undergoes significant volume changes on electrochemical cycling. Additives, such as Al_2O_3 [24–27] and $Mg_{0.6}Ni_{0.4}O$ [9,20], act as electrolyte absorbents, locally limiting the polysulphide shuttle effect. The addition of $Mg_{0.6}Ni_{0.4}O$ additive to S/PAN composite materials has successfully demonstrated performance improvement in Li/S batteries. Recently another conductive polymer, polyaniline, has shown promising results as a conductive support for S cathodes, it also has practical advantages owing to its high environmental stability, high electrical conductivity, and easy synthesis. Here we examine, for the first time known to the authors, the effect of polyaniline (PANI) with both $Mg_{0.6}Ni_{0.4}O$ and Al_2O_3 additives on the performance of the lithium sulphur battery.

2. Experimental section

2.1. S-composites preparation

The $Mg_{0.6}Ni_{0.4}O$ synthesis was carried out by a self-propagating high temperature synthesis method, as described in previous work of the authors [12]. Sulphur (Sigma-Aldrich, 100 mesh particle size powder), polyaniline (Sigma-Aldrich, emeraldine salt composite, 20 wt.% polyaniline on carbon black) and $Mg_{0.6}Ni_{0.4}O$ (as prepared) or Al_2O_3 (Sigma Aldrich, nanopowder, <50 nm particle size (TEM)) were mixed in the mass ratio of 4:1:0.25 by wet ball milling at 800 rpm for 3 h with ethanol as a dispersant. The sulphur/polyaniline binary composite was mixed in the same way in the mass ratio of 4:1.

The S-composites were dried in an air-ventilated oven for 2 h at 60 °C to remove the remaining ethanol; and finally heat treated in two subsequent steps for 3 h at 160 °C followed by for 3 h at 300 °C under argon in a tube furnace.

2.2. S-composites characterization

The sulphur content in the S-composites was analysed using chemical analysis (CHNS, Vario Micro Cube, Elementar). The crystalline phase of $Mg_{0.6}Ni_{0.5}O$ powder was analysed using powder X-ray diffraction (XRD, a Bruker-AXS D4 system Philips Analytical PW-1710) with Mo radiation at a scanning speed of 2°/min.

The nitrogen adsorption method (BET, Micromeritics, Gemini 2370) was used for specific surface area measurements. Before measurement of pure $Mg_{0.6}Ni_{0.5}O$ and Al_2O_3, the samples were degassed at 150 °C in a vacuum line following a standard protocol, but owing to the volatility of the sulphur, no pre-treatment of the S composites was used. Therefore, due to the possibility of water entrapment, and/or pore blockage in the micropores, the obtained values could represent the lower estimates; however, these results demonstrate the trends for comparison between different S composites.

Scanning electron microscopy (SEM, JEOL JSM-840 or Zeiss EVO10) was employed to investigate the particle morphology. In order to increase the contrast and the quality of images, the samples were sputter coated with a 3 nm layer of gold prior to analysis. Samples after charge/discharge tests were washed with 40 mL of solvent composed by TEGDME (to remove soluble components) prior to SEM and EDS measurements.

Thermal gravimetric analysis (TGA) measurements were carried out (Q500, TA Instruments) for a temperature range of 25 to 600 °C to determine the thermal properties of the S composites.

2.3. Cell assembly and electrochemical characterization

The electrodes were prepared by mixing the active material (S/PANI, S/PANI/Al_2O_3, S/PANI/$Mg_{0.6}Ni_{0.5}O$ composites) with Ketjenblack (Ketjenblack 300, AkzoNobel), poly(vinylidene fluoride) (PVDF, MTI Inc.) in a mass ratio of 80:10:10, respectively, in N-methyl-2-pyrrolidone (NMP, MTI Inc.). The resultant slurry was uniformly spread onto Ni foam (≥95% purity, 96% porosity Goodfellow Cambridge Ltd.) discs with a diameter of 1.6 cm and dried at 70 °C for 12 h in air-ventilated oven. After this the electrodes were pressed by a hydraulic press at 5 MPa to enhance contact between the active material and Ni foam current collector. The Ni foam current collector was chosen instead of aluminium foil due to its three-dimensional structure that gives higher mass loading of active material per unit area. The thickness achieved was about 60 μm, and the mass of the electrodes were in a range of 8–10 mg cm^{-2}, which gives a resultant areal capacity of over 2 mA cm^{-2}. For a fair comparison the electrodes examined were of equal mass.

Electrochemical tests of the S/composites were performed using the coin-type cells (CR2032) with lithium metal foil as the counter electrode. CR2032 coin-type cells were assembled in a glove box filled

with high purity argon (99.9995% purity) by sandwiching a polypropylene separator (Celgard, MTI Inc.) between the composite cathode and lithium anode and using 1 M lithium hexafluorophosphate ($LiPF_6$) in tetra(ethylene glycol) dimethyl ether (TEGDME) as the electrolyte.

Galvanostatic charge/discharge and cyclic voltammetry (CV) were used to test the electrochemical properties of the cathode materials. CV was conducted using a potentiostat (Gamry, Reference 3000) at a scan rate of 0.05 mV s^{-1} between 1 and 3 V vs. Li$^+$/Li. The cells were cycled galvanostatically using a multichannel battery tester (BT-2000, Arbin), in the range 1 to 3 V vs. Li$^+$/Li at 0.1 C. Impedance measurements were conducted by means of potensiostat (Gamry, Reference 3000). The frequency of AC impedance was varied from 0.1 Hz to 1 MHz with applied voltage amplitude of 5 mV. Applied currents and specific capacities were calculated on the basis of the mass of S in the cathode. All electrochemical measurements were performed at room temperature.

3. Results and discussion

3.1. Physical characterization of S-composites

Fig. 1 shows the XRD pattern of $Mg_{0.6}Ni_{0.5}O$ powder. The diffraction peaks at $2\Theta = 6°, 16.7°, 19.5°, 27°, 6°, 32.4°, 34°$ were attributed to (001), (111), (200), (220), (311), (222) planes of the face centred cubic structure of $Mg_{0.6}Ni_{0.5}O$. This shows that the synthesized material is $Mg_{0.6}Ni_{0.5}O$ powder. The structure of the $Mg_{0.6}Ni_{0.5}O$ was also studied by TEM (Fig. 2). The TEM image and particle size distribution analysis derived from it (in Fig. 2 a and b) show that $Mg_{0.6}Ni_{0.5}O$ has nanostructure which consists of the particles less than 30 nm, the mean diameter $d_p = 20$ nm.

The composition of the sulphur composites prepared in this study is given in Table 1.

Chemical analysis has shown ca. 30% of sulphur loss during the heat treatment process (see Table 1).

In Table 2 the BET specific area of the S-composites is given: S/PANI/ $Mg_{0.6}Ni_{0.4}O$ has the highest BET area of 18.1 m^2 g^{-1} among the S-composites prepared in this work.

The BET isotherm obtained was of type 1, which is known to correspond to macroscopic surface area: because of the sulphur content of the composite, and its tendency to sublime at elevated temperatures, it is not possible to carry out the heat pre-treatment typical of BET measurements, without the risk of damaging the analysis equipment. It is expected therefore that adsorbed water, particularly in the micropores of the composite material may still be present and affects the obtained results and values. By contrast, Zhao et al. [19] report BET analysis for a PANI/C (Sigma-Aldrich Co) composite material, the type 4 BET isotherm was obtained, indicative of a mesoscopic pore structure within the macroscopic particles.
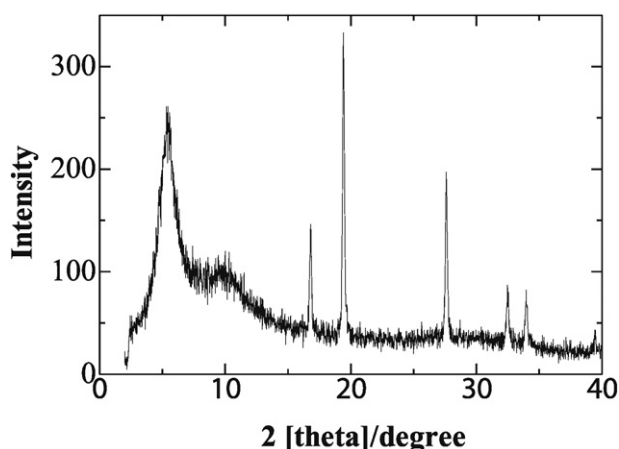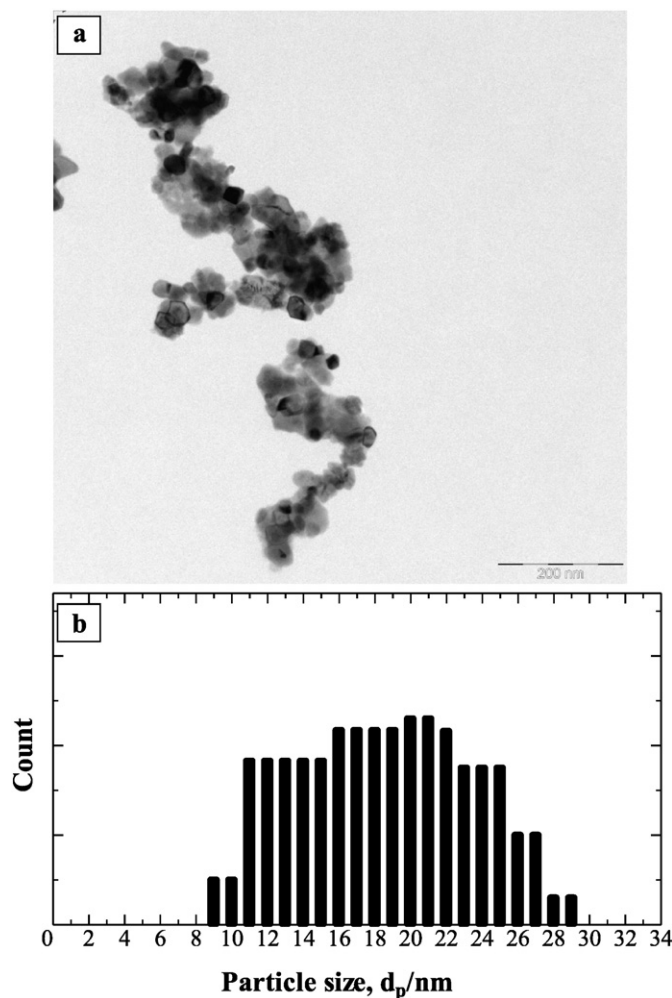

Fig. 2. a) TEM image of $Mg_{0.6}Ni_{0.5}O$; b) particle size distribution.

The morphology of the fresh S composites is presented in Fig. 3. It can be seen that the S/PANI composite (Fig. 3a) has an agglomerated plate-like structure. The addition of metal oxides changes the morphologies of the composites (Fig. 3b and c), resulting in a number of irregular pores and rougher surfaces as it mainly consisted of smaller primary particles with different diameters, leading to the higher specific surface area. The formation of a mesoporous structure will favour the electrolyte penetration into the electrodes, enhancing ion transport and charge transfer. It was also observed that the Al_2O_3 addition had a smaller influence on the composite morphology than that of $Mg_{0.6}Ni_{0.4}O$. The S/PANI/Al_2O_3 composite has morphology similar to that of the bare S/PANI composite, but with a much smaller pore diameter. The porous microstructure of the pure PANI material is shown in Fig. 3 d. The elemental mapping presented in Fig. 6 shows that both $Mg_{0.6}Ni_{0.4}O$ and Al_2O_3 were uniformly mixed with sulphur and polyaniline, and no sulphur accumulation was observed on the surface.

Fig. 1. XRD pattern of the as prepared $Mg_{0.6}Ni_{0.4}O$.

Table 1
List of S-composites.

S composite	Initial mass ratio respectively	Initial S content, mass %	S content after the heat treatment by CHNS, mass %
S/PANI	4:1	80%	42.9
S/PANI/$Mg_{0.6}Ni_{0.4}O$	4:1:0.25	≈76%	41.8
S/PANI/Al_2O_3	4:1:0.25	≈76%	41.6

Table 2
BET area of the samples.

Sample name	BET area ($m^2\,g^{-1}$)
$Mg_{0.6}Ni_{0.4}O$ as-prepared	54.0
Al_2O_3	144.0
S/PANI	11.4
S/PANI/$Mg_{0.6}Ni_{0.4}O$	18.1
S/PANI/Al_2O_3	13.4

The thermogravimetric analysis (TGA) of S-composites and bare sulphur powder are shown in Fig. 4; the mass loss due to the sulphur evaporation occurs in the temperature range from 200 to 350 °C; it can be seen that the bare sulphur was burned completely at 330 °C, the composites undergo a further mass loss due to decomposition of other components in the samples, in agreement with the literature data [17]. The mass losses detected from the TGA data agree with the CHNS results on the S content in the heat treated samples. For S composites the gradual pattern of the curves demonstrated that sulphur was well trapped within the internal pores of PANI. The first mass loss at around 200 °C could also be associated with the decomposition of sulphonic acid and a part of amino– sulphur interaction. It can be seen that the thermal behaviour of the sample with $Mg_{0.6}Ni_{0.4}O$ was different from that of other composites: a second plateau from 280 to 350 °C could be observed. This could be due to the morphology difference caused by the $Mg_{0.6}Ni_{0.4}O$ additive and formation of the internal pore space: so the sample contains two types of sulphur; one closer to the surface (easy to evaporate) and another one trapped in the internal pore space (consequently more difficult to evaporate).

sFig. 5 shows the SEM images of the initial (i) and cycled (ii) composite cathodes. It can be seen that significant morphology changes occur upon cycling for the S/PANI (Fig. 5a) binary composite.

Although the sample with nanoparticles of Al_2O_3 had an initial structure different from that of the S/PANI system, with a highly porous morphology and relatively dense surface, upon cycling this composite underwent noticeable morphology changes and became similar to
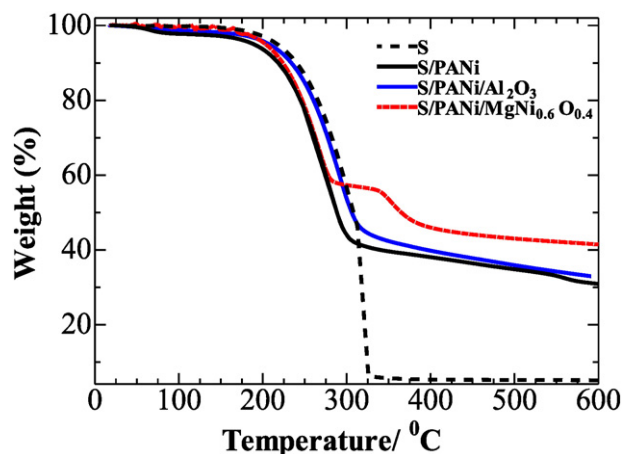

Fig. 4. Thermogravimetric curves of S and S-composites.

that of the S/PANI composite, with evidence of active material agglomeration (Fig. 5b). The active material agglomeration in the studied systems suggested its separation from the conductive agent, thus the separated non-conductive parts of the active material did not appear to take part in any further electrochemical operations, resulting in lower sulphur utilization and a rapid capacity loss.

In contrast, the morphology of S/PANI/$Mg_{0.6}Ni_{0.4}O$ (Fig. 5c) did not change remarkably upon cycling; intact particles were bound together in the cycled cathode and retained a morphology similar to that of the initial composite cathode.

3.2. Electrochemical properties of S-composite cells

Fig. 7 presents the cyclic voltammograms (CV) of a lithium–sulphur cell with the S/PANI, S/PANI/$Mg_{0.6}Ni_{0.4}O$ and S/PANI/Al_2O_3 composite

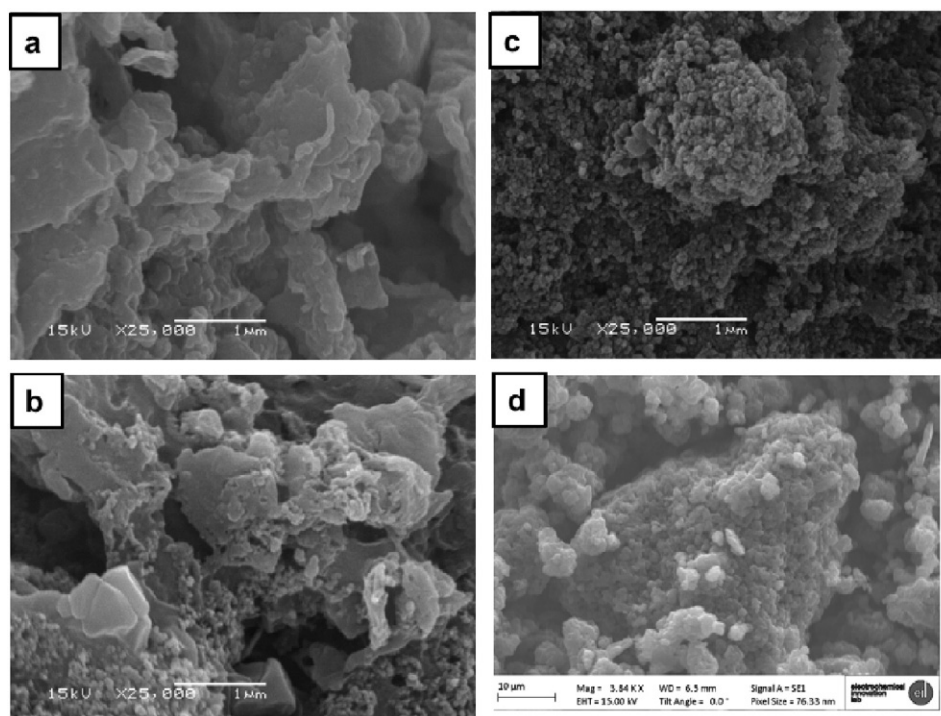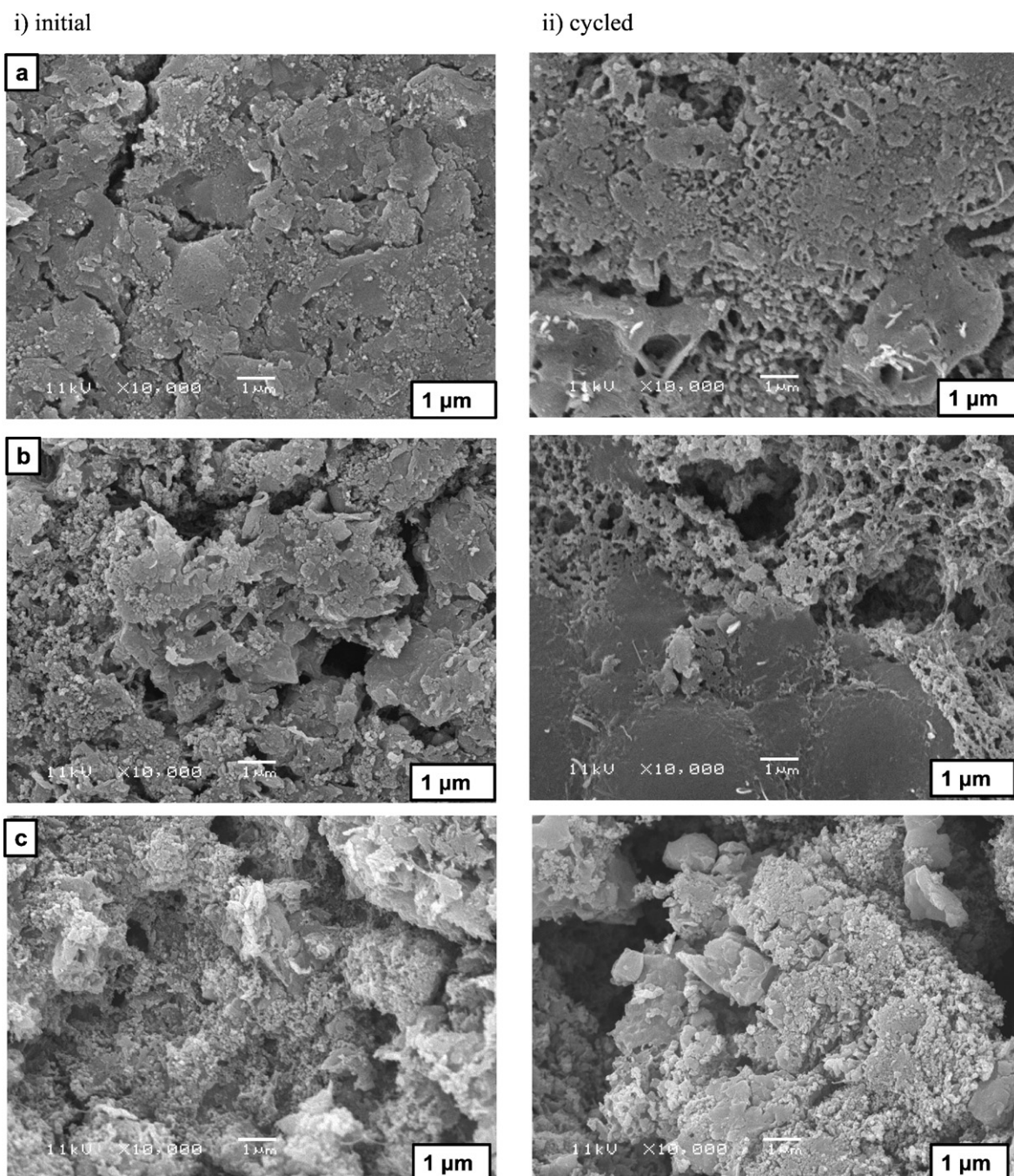**Fig. 3.** SEM images of the composites: a) S/PANI; b) S/PANI/Al_2O_3; c) S/PANI/$Mg_{0.6}Ni_{0.4}O$; d) pure PANI.

i) initial   ii) cycled

Fig. 5. SEM images of electrodes before (i) and after 25 cycles (ii) a) S/PANI; b) S/PANI/Al_2O_3; c) S/PANI/$Mg_{0.6}Ni_{0.4}O$;

cathodes, which exhibit different features of reversible operation of a Li/S cell.

A cathodic peak for S/PANI composite located at 2.4 V was attributed to the reduction of elemental sulphur into soluble polysulphides (Li_2S_x, $2 < x \leq 8$), whereas the following reduction peak around 2.0 V was assigned to the further reduction of polysulphides to insoluble polysulphides (Li_2S_2, Li_2S). The peaks, observable as shoulders in the CV at ca. 2.25 V and 2.5 V are thought to be due to inter-reaction between soluble polysulphides (the poly-sulphide shuttle effect).

During the reverse sweep, the CV shows that a sharp anodic peak ca. 2.35 V was assigned to a reversible conversion of polysulphides to sulphur. Thus the electrochemical behaviour of the S/PANI composite followed typical sulphur cathode oxidation/reduction trends in lithium batteries.

Similar trends were observed in the CV curves of the S/PANI/Al_2O_3 composite, although the redox peaks of the S/PANI/Al_2O_3 cathode were slightly shifted towards each other, which could be due to the lower polarization. No additional peaks were associated with the Al_2O_3, indicating that this additive was electrochemically inactive in the selected potential region.

Likewise, the $Mg_{0.6}Ni_{0.4}O$ additive was not electrochemically active in the selected voltage region. On the initial voltage cycle for this system there was a pronounced reduction process (Fig. 8), which was similar to that observed in previous work of some of the authors [12] for the S/PAN/$Mg_{0.6}Ni_{0.4}O$ composite. It is believed that this process is due to the side reactions and the SEI formation. It is also observed in the galvanostatic charge–discharge test, the initial discharge profile (Fig. 9) is different from the subsequent profiles, suggesting that there is a
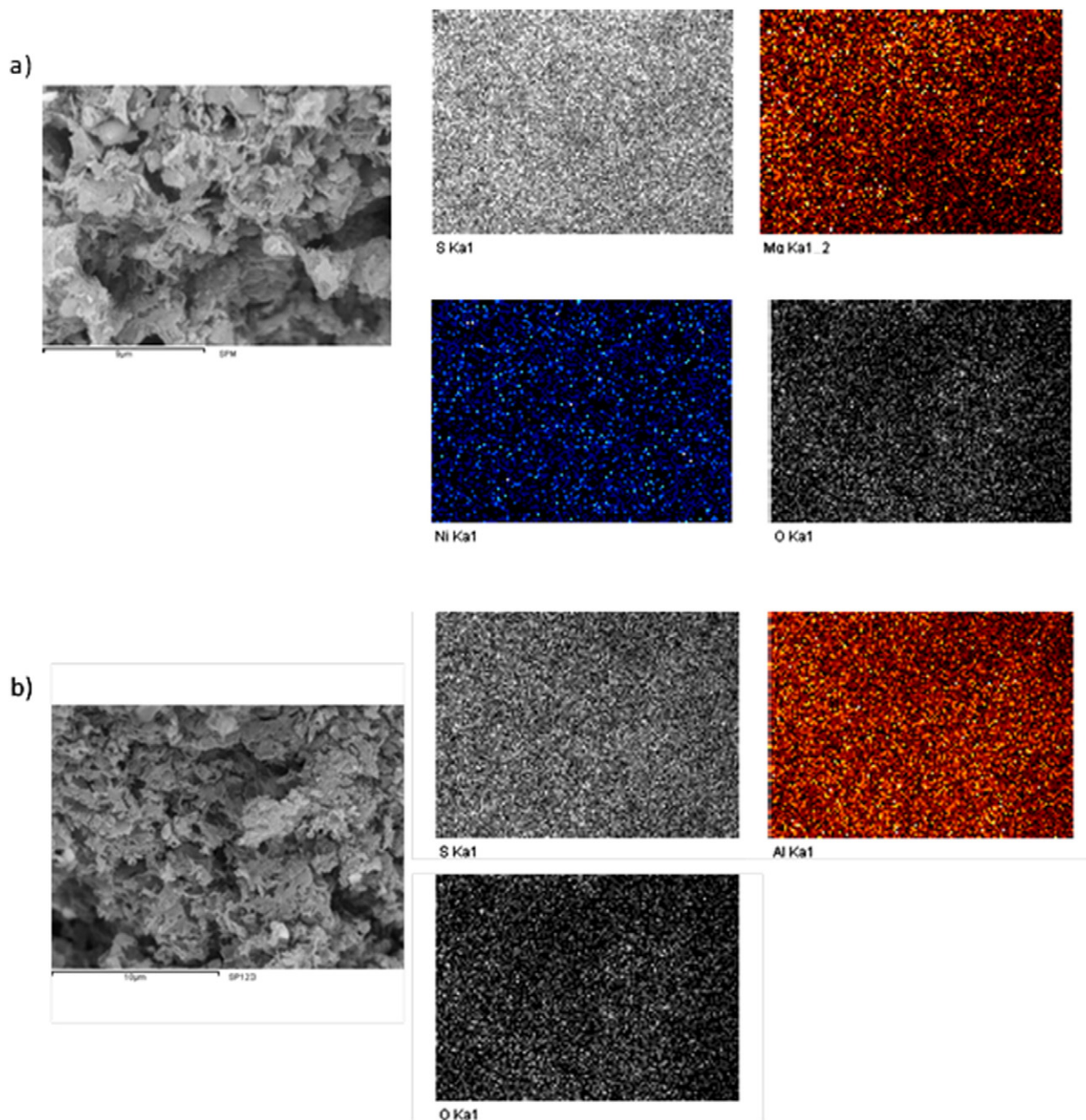
Fig. 6. EDS elemental mapping of a) S/PANI/Mg$_{0.6}$Ni$_{0.4}$O; b) S/PANI/Al$_2$O$_3$;

pronounced polarization between the reduction and the oxidation peaks. It is also noteworthy that the high potential polarization caused the single broad cathodic and anodic peaks representing overlapped processes: between soluble, high order polysulphides (i.e. Li2Sn, n ≥ 3) and insoluble, low order polysulphides (Li$_2$S$_n$, n ≤ 2), inherent to the Li/S battery [6,31,32].

The CV of S/PANI/Mg$_{0.6}$Ni$_{0.4}$O composite compared to S/PANI and S/PANI/Al$_2$O$_3$ composites has larger cathodic and anodic current density peaks, suggesting that this composite has a higher discharge capacity and active sulphur utilization (c.a. 90%), which is in agreement with the charge–discharge data. These effects might also have been due to the adsorbing and catalytic activity of the Mg$_{0.6}$Ni$_{0.4}$O additive. The additive acted as an adsorbent of lithium polysulphides, reducing the shuttle effect of the polysulphides, and, as shown by the SEM results, the additive prevented agglomeration of the active material and preserved

the higher conductivity of the sample. The CV data comply with that previously reported in the literature [12].

Fig. 9 shows the initial galvanostatic charge–discharge profiles of the S/PANI, S/PANI/Al$_2$O$_3$ and S/PANI/Mg$_{0.6}$Ni$_{0.4}$O composites. It can be seen that the Mg$_{0.6}$Ni$_{0.4}$O and Al$_2$O$_3$ additives enhanced the sulphur utilization in the cathode, and these composites exhibited much higher capacity than the 'bare' S/PANI system. Furthermore, the S/PANI/Mg$_{0.6}$Ni$_{0.4}$O composite cathode exhibited the highest capacity among the studied systems. It should be noted that at the initial discharge the S/PANI/Mg$_{0.6}$Ni$_{0.4}$O composite exhibited a continuous voltage decline which is a known phenomenon for sulphur composite cathodes and attributed to the side reactions of a solid electrolyte interphase (SEI) formation [9,28,29]. Starting from the following cycle, this composite exhibited the typical Li/S potential profile features associated with the reversible reaction of Li and S. The short discharge plateau about 2.5 V is related
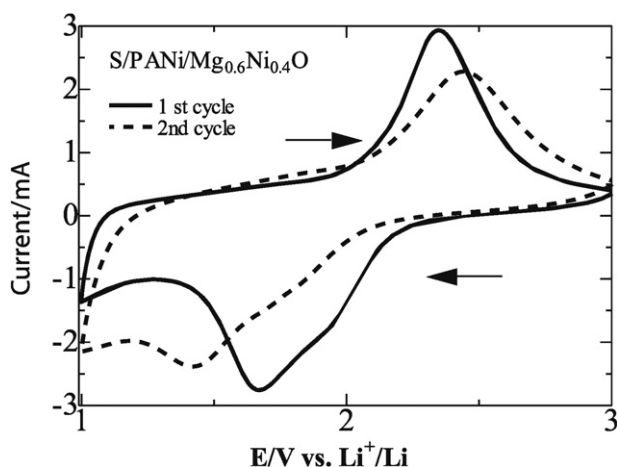
Fig. 7. CV curves of a lithium cell with $S/PANI/Mg_{0.6}Ni_{0.4}O$, $S/PANI/Al_2O_3$ and S/PANI composite cathodes; cycling rate 0.05 mV/s.

to the formation of higher-order soluble lithium polysulphides (Li_2S_n, $n \geq 4$), followed by a plateau around 2.0 V, which reflects the transition of the polysulphides into lithium sulphide Li_2S. The kinetics of the latter reaction were slower than that of the polysulphide formation, which agrees with the literature data [33] and the CV data obtained in this work.

Another observation for the $S/PANI/Mg_{0.6}Ni_{0.4}O$ composite compared with the S/PANI and $S/PANI/Al_2O_3$ counterparts is a reduction of the charge and discharge voltage gap; this reflects a reduced polarization in the system, and has been reported in previous work for the S/ polyacrylonitrile/$Mg_{0.6}Ni_{0.4}O$ composite [9].

Fig. 9d shows the composite cathodes' cyclability in a lithium half-cell. It can be seen that the S/PANI composite exhibited an initial discharge capacity of ca. 1025 mA h g^{-1} and the cell loses about 75% of this value within the first 20 cycles, with a stabilized discharge capacity of 300–400 mA h g^{-1}. For comparison, the S/PANI-NHT composite was prepared by simple wet ball milling of sulphur and PANI at room temperature with no heat treatment step (catergorised here as NHT). As seen in Fig. 9d, the cell with S/PANI exhibited a slightly better discharge capacity than the cell with S/PANI-NHT, clearly indicating that heat treatment of S composites gave better electrochemical performance. This could be attributed to the cross-linking reactions between the conducting polymer and sulphur occurring during the heat treatment, so sulphur could have been stored in composites not only by physical
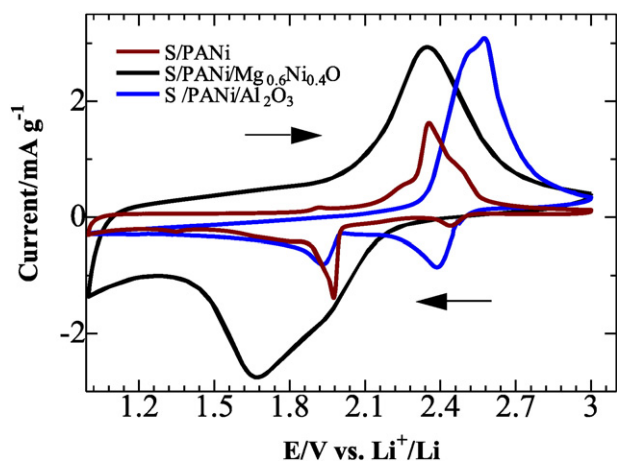
adsorption but by chemical bonding, as was shown by Zhao et al. for S ternary composite with PANI [19].

It can be seen from Fig. 9d that the initial discharge capacity of the S/ $PANI/Al_2O_3$ cathode is 1392 mA h g^{-1} and it retained a capacity of 612 mA h g^{-1} after 100 cycles.

The $S/PANI/Mg_{0.6}Ni_{0.4}O$ composite delivered a capacity of 1448 mA h g^{-1} at the initial cycle, and 1220 mA h g^{-1} at the following cycle, indicating a high sulphur utilization (about 89.5%). The cell with this cathode retained ca. 48% of the initial value after 100 cycles, exhibiting about 772 mA h g^{-1}.

Electrochemical impedance spectroscopy (EIS) was employed to investigate the effect of the $Mg_{0.6}Ni_{0.4}O$ and Al_2O_3 additives on the electrochemical behaviour of the S/PANI composite cathode. Fig. 10 shows the EIS spectra of fresh lithium cells with and without the oxide additives. Equivalent circuit analysis for each composite was conducted, and shown to be in agreement with Zhang et al. Ref. [12], as shown in Fig. 10 in the inset. In this model, R_1 is the internal resistance of the tested battery, R_2 and R_3 represent the passivation film and charge–discharge transfer, Q_1 and Q_2 are the constant phase elements responsible for the double layer capacitance and W is the Warburg resistance related to the lithium diffusion process. The fitted impedance parameters are listed in the Table 3. It can be seen that for all the composites the Nyquist plots represent the Randles-like equivalent circuit behaviour, and comprise of depressed semicircles in the high-to-medium frequency region due to the charge transfer resistance, followed with an inclined linear region (the so-called Warburg impedance) at low frequency due to the ion diffusion impedance within the cathode [28,30]. It can be seen that the charge transfer semicircles ($R_2 + R_3$) for both composites with the metal oxide additives (98.15 Ω and 88.23 Ω respectively for $S/PANI/Al_2O_3$ and $S/PANI/Mg_{0.6}Ni_{0.4}O$) were much smaller than the no-additive S/PANI system (208.06 Ω), with the $Mg_{0.6}Ni_{0.4}O$ composite exhibiting the lowest charge transfer resistance.

4. Conclusions

Sulphur/polyaniline composites were prepared by a simple ball milling with Al_2O_3 and $Mg_{0.6}Ni_{0.4}O$ as metal oxide additives followed by heat treatment. Addition of $Mg_{0.6}Ni_{0.4}O$ led to a reduction in polarization (charge transfer impedance) and improved performance. For the ternary composite $S/PANI/Mg_{0.6}Ni_{0.4}O$/, a specific capacity of 1448 mA h g^{-1} was delivered in the initial discharge and a reversible capacity of ~900 mA h g^{-1} was obtained after 10 cycles. It was shown that the addition of $Mg_{0.6}Ni_{0.4}O$ to S/PANI composite improved the composite morphology upon cycling, kinetics and electrochemical performance of the cell. The addition of Al_2O_3 also improved the S/PANI composite's electrochemical performance, delivering an initial discharge capacity of 1392 mA h g^{-1} with the retained capacity of 612 mA h g^{-1} after 100 cycles, which was lower than for the $Mg_{0.6}Ni_{0.4}O$ additive.

The results indicate that the metal oxide nano-composite additives enhanced the electrochemical performance of the S electrodes. The composites with metal oxide additives had a more homogenous morphology compared with the initial S/PANI cathode. However, the alumina additive had a lesser enhancement effect on the sulphur/polyaniline composite compared with $Mg_{0.6}Ni_{0.4}O$ additives.

Conflict of interest

There is no conflict of interest.

Acknowledgements

Fig. 8. CV curves of a lithium cell with S/PANI, $S/PANI/Al_2O_3$ and $S/PANI/Mg_{0.6}Ni_{0.4}O$ composite cathodes; cycling rate 0.05 mV/s.
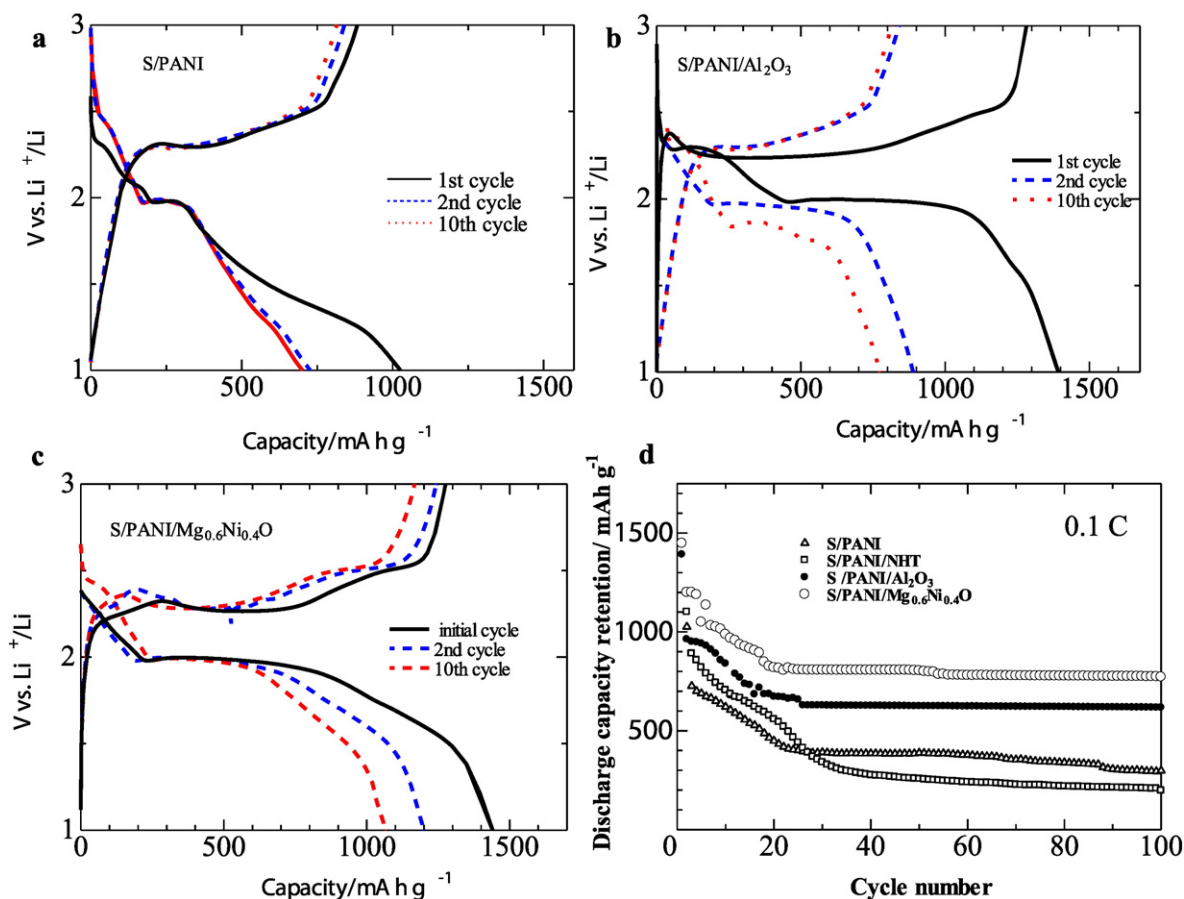
Fig. 9. Charge–discharge profiles of lithium cells with a) S/PANI, b) S/PANI/Al_2O_3 and c) S/PANI/$Mg_{0.6}Ni_{0.4}O$ composites cathodes at 0.1 C; d) cyclability of lithium cells with S/PANI, S/PANI-NHT, S/PANI/Al_2O_3 and S/PANI/$Mg_{0.6}Ni_{0.4}O$ composites cathodes at 0.1 C.
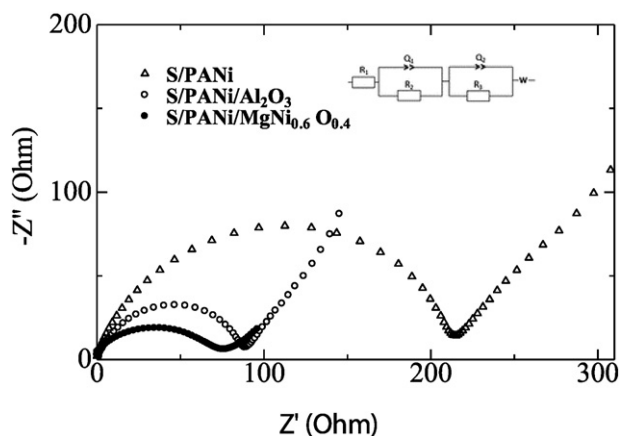

Fig. 10. EIS impedance plots of fresh lithium cells with the S/PANI, S/PANI/Al2O3 and S/PANI/Mg0.6Ni0.4O cathodes.

Table 3
The EIS simulation parameters.

Cathodes	R_1 (Ω)	R_2 (Ω)	R_3 (Ω)	Q_1 (μF)	Q_2 (μF)	W (Ω s$^{-1/2}$)
S/PANI	1.99	82.26	125.8	1.566	3.233	86.04
S/PANI/Al_2O_3	2.9	56.65	41.5	5.091	2.431	58.96
S/PANI/$Mg_{0.6}Ni_{0.4}O$	1.76	51.66	36.57	7.345	0.677	21.08

References

[1] H. Kawamoto, Science and Technology Trends 36/July 20, 2011.
[2] P. Bruce, S. Freunberger, Nat. Mater. 11 (2012) 19.
[3] P.U. Munshi, J. Pichel, E.S. Kwei, P. Jaffray, Invest. Res. (2009) 41.
[4] Y. Yang, G. Zheng, Y. Cui, Chem. Soc. Rev. 42 (2013) 3018.
[5] L. Chen, L.L. Shaw, J. Power Sources 267 (2014) 770.
[6] X. Ji, L.F. Nazar, J. Mater. Chem. 20 (2010) 9821.
[7] D.-W. Wang, Q. Zeng, G. Zhou, L. Yin, F. Li, H.-M. Cheng, I.R. Gentle, G.Q.M. Lu, J. Mater. Chem. A 1 (2013) 9382.
[8] D. Kumar, R.C. Sharma, Eur. Polym. 34 (1998) 1053.
[9] J. Jagur-Grodzinski, Polym. Adv. Technol. 13 (2002) 615.
[10] J. Li, K. Li, M. Li, D. Gosselink, Y. Zhang, P. Chen, J. Power Sources 252 (2014) 107.
[11] L. Wang, X. He, J. Li, M. Chen, J. Gao, C. Jiang, Electrochim. Acta 72 (2012) 114.
[12] Y. Zhang, Y. Zhao, A. Yermukhambetova, Z. Bakenov, P. Chen, J. Mater. Chem. A 1 (2013) 295.
[13] X. Liang, Y. Liu, Z. Wen, L. Huang, X. Wang, H. Zhang, J. Power Sources 196 (2011) 6951.
[14] Y. Fu, Y.-S. Su, A. Manthiram, J. Electrochem. Soc. 159 (2012) A1420.
[15] Y. Zhang, Z. Bakenov, Y. Zhao, A. Konarov, T.N.L. Doan, M. Malik, T. Paron, P. Chen, J. Power Sources 208 (2012) 1.
[16] M. Sun, S. Zhang, T. Jiang, L. Zhang, J. Yu, Electrochem. Commun. 10 (2008) 1819.
[17] J. Wang, J. Chen, K. Konstantinov, L. Zhao, S.H. Ng, G.X. Wang, Z.P. Guo, H.K. Liu, Electrochim. Acta 51 (2006) 4634.
[18] F. Wu, J. Chen, R. Chen, S. Wu, L. Li, S. Chen, T. Zhao, J. Phys. Chem. C 115 (2011) 6057.
[19] X. Zhao, J.-K. Kim, H.-J. Ahn, K.-K. Cho, J.-H. Ahn, Electrochim. Acta 109 (2013) 145.
[20] L. Xiao, Y. Cao, J. Xiao, B. Schwenzer, M.H. Engelhard, L.V. Saraf, Z. Nie, G.J. Exarhos, J. Liu, Adv. Mater. (Deerfield Beach, Fla.) 24 (2012) 1176.
[21] J. Jin, Z. Wen, G. Ma, Y. Lu, K. Rui, Solid State Ionics 262 (2013) 170.
[22] G.-C. Li, G.-R. Li, S.-H. Ye, X.-P. Gao, Adv. Energy Mater. 2 (2012) 1238.
[23] M.-S. Song, S.-C. Han, H.-S. Kim, J.-H. Kim, K.-T. Kim, Y.-M. Kang, H.-J. Ahn, S.X. Dou, J.-Y. Lee, J. Electrochem. Soc. 151 (2004) A791.

[24] X. Han, Y. Xu, X. Chen, Y.-C. Chen, N. Weadock, J. Wan, H. Zhu, Y. Liu, H. Li, G. Rubloff, C. Wang, L. Hu, Nano Energy 2 (2013) 1197.
[25] Z. Zhang, Y. Lai, Z. Zhang, K. Zhang, J. Li, Electrochim. Acta 129 (2014) 55.
[26] K. Dong, S. Wang, H. Zhang, J. Wu, Mater. Res. Bull. 48 (2013) 2079.
[27] Y.J. Choi, B.S. Jung, D.J. Lee, J.H. Jeong, K.W. Kim, H.J. Ahn, K.K. Cho, H.B. Gu, Phys. Scr. T129 (2007) 62.
[28] Y. Zhang, L. Wang, A. Zhang, Y. Song, X. Li, H. Feng, X. Wu, P. Du, Solid State Ionics 181 (2010) 835.
[29] X.Z. Ma, B. Jin, H.Y. Wang, J.Z. Hou, X.B. Zhong, H.H. Wang, P.M. Xin, J. Electroanal. Chem. 736 (2015) 127.
[30] Y. Zhang, Z. Bakenov, Y. Zhao, A. Konarov, T.N.L. Doan, K.E.K. Sun, A. Yermukhambetova, P. Chen, Powder Technol. 235 (2013) 248.
[31] A. Manthiram, Y. Fu, S.-H. Chung, C. Zu, Y.-S. Su, Chem. Rev. 114 (23) (2014) 11751.
[32] J. Yan, X. Liu, M. Yao, X. Wang, T.K. Wafle, B. Li, Chem. Mater. (2015) 5080.
[33] Y.-X. Yin, S. Xin, Y.-G. Guo, L.-J. Wan, Angew. Chem. Int. Ed. Engl. 52 (2013) 13186.